Imagem

Identificação do Autor

TÍTULO

Dissertação de Mestrado em Engenharia [Mecânica]
na Especialidade de [Energia e Ambiente/ Produção e Projecto]

Data/Ano

· U C ·

UNIVERSIDADE DE COIMBRA

• U C •

FCTUC FACULDADE DE CIÊNCIAS
E TECNOLOGIA
UNIVERSIDADE DE COIMBRA

DEPARTAMENTO DE
ENGENHARIA MECÂNICA

Study of the traction curves

Submitted in Partial Fulfilment of the Requirements for the Degree of Master in Mechanical Engineering in the speciality of Production and Project

Estudo das curvas de tração

Author

João Ricardo de Almeida Ganhoto

Advisors

Professor Doutor Amílcar Lopes Ramalho

Professor Doutor François Robbe-Valloire

Jury

President	**Professor Doutor Fernando Jorge Ventura Antunes** **Professor Auxiliar da Universidade de Coimbra**
Vowel	**Professor Doutor [Luis Manuel** **[Investigador Auxiliar] da Universidade de Coimbra**
Advisor	**Professor Doutor Amílcar Lopes Ramalho** **Professor Associado c/ Agregação da Universidade de Coimbra**

Institutional Collaboration

supméca

Institut Superieur
Mecánique de Paris

Coimbra, June, 2018

“Who learns to get out of its comfort zone will fall and fail.
But in the end, that has the purpose of breaking the eggshell
which was hiding the way out, and preventing him to fly away.. “
Miguel Panão

[Os trabalhos escolares são provas para o carácter, não para a inteligência. Quer se trate de ortografia, de poesia ou de cálculo, está sempre em causa aprender a querer.]
[Alain, em Les Idées et les Âges, 1927.]

To my parents.

[Página facultativa. Apagar se não aplicável.]

ACKNOWLEDGEMENTS

This short space reserved to the acknowledgements will not let me to thank everybody that have crossed and helped me throughout my Master Degree in Mechanical Engineering, with

[Remover se necessário para garantir que o Resumo inicia numa página ímpar]

Abstract

The main objective of the work presented is the development of models, algorithms and numerical methods to be used in the simulation of the deep drawing process. The intention is to increase the robustness, precision and numerical efficiency of simulation codes. Developments are implemented and tested in a finite element code named DD3IMP.]

Keywords [Keyword 1], [Keyword 2], [Keyword 3], [Keyword 4], [Keyword 5], [Keyword 6].

[Remover se necessário para garantir que o Índice inicia numa página ímpar]

Resumo

O objetivo principal deste trabalho é fazer um estudo teórico, usando um modelo de contacto proposto por , que visa validar, ou não, testes realizados num tribómetro de disco duplo, no Institut Supérieur de Mecánique de Paris (SUPMECA), comparando, ambos os resultados, como a teoria linear de Kalker.

Para tal, fez-se um estudo alongado sobre o contacto entre superfícies cilíndricas lisas e rugosas, carregadas com diferentes tipos de esforços, começando no mais simples, acabando no mais complexo. Muitas das avaliações feitas neste trabalho, tiveram por base modelos já existentes que serão corretamente citados *à posteriori*.

No final irá, então, fazer-se a comparação de ambos os resultados para ver se se chega a um consenso quanto à validade das experiencias feitas.

Palavras-chave: Mecânica de contacto, Atrito, Contacto cilindro-cilindro, [Palavra-chave 4], [Palavra-chave 5], [Palavra-chave 6].

[Remover se necessário para garantir que o Abstract inicia numa página ímpar]

Contents

[LIST OF FIGURES] [(REMOVER SE NÃO APLICÁVEL)]

[Remover se necessário para garantir que o Índice de Tabelas inicia numa página ímpar]

[Remover se não aplicável.]

[LIST OF TABLES] [(REMOVER SE NÃO APLICÁVEL)]

[Remover se necessário para garantir que a Simbologia e Siglas inicia numa página ímpar]

[Remover se não aplicável.]

[SIMBOLOGY] AND [ACRONYMS] [(REMOVER SE NÃO APLICÁVEL)]

[Simbology] [(remover se não aplicável)]

A– Area.

a– Contact half width.

b– Ellipse's minor measure.

C– Modulus of rigidity.

E – Young's modulus.

E' – Equivalent Young's modulus.

F_N– Normal force.

F_{ns}– Nominal static threshold.

F_S– Static friction force.

F_T– Tangential force.

k– Stiffness.

k_a, k_b– Constants.

L– Length.

m– Mass.

n_i– Number of contacting points.

p– Periodicity.

$P(x)$– Pressure.

P_0– Maximum pressure.

R– Radius.

R'– Equivalent radius.

$\mathrm{R_a}$ – Arithmetic mean surface roughness.

$\mathrm{R_{asp}}$ – Asperity radius.

R_q– Root mean square average surface roughness.

V – Linear velocity.

ΔV – Sliding velocity.

w – Angular velocity.

Δw – Angular velocity of roll.

V_r– Rolling velocity.

x, z– Contact position.

$\bar{\xi}$– Sliding rate.

μ – Friction coefficient.

μ_S– Static friction coefficient.

ν– Poisson's ratio.

ϕ – Angle between planes.

δ– Displacement.

[Acronyms] [(remover se não aplicável)]

SR – Sliding rate.

SUPMECA – Institut Superieur Mecánique de Paris.

[Remover se necessário para garantir que o Primeiro Capítulo inicia numa página ímpar]

1. INTRODUCTION

This first chapter, as the name implies, is reserved for an initial briefing about this dissertation main theme.

The goal of this work is to study the contact between objects in rolling/sliding situation, and at the same measuring the friction coefficient evolution while comparing it to Kalker's Linear Theory. After this embryonic stage, it will be possible to deal with real experiences made in a twin disk tribometer, in the host university, Institut Superieur Mecánique de Paris.

I will firstly do a brief synopsis about the perception and the origin of the loss of energy in a certain system. Here, it is shown the main background already known about the immense subject that is tribology.

1.1. Historical review

First things first, what is friction? By definition, friction is a force which make it difficult for an object to slid over or move over another, and so, this resistive force has the same orientation, but has an opposite direction. This force is intimately connected to a coefficient, known as friction ratio or coefficient of friction, μ, which can be calculated by doing the quotient between tangential and normal forces on the contact:

$$\mu = \frac{F_T}{F_N} \tag{1.1}$$

In our daily routine many, or even infinite, are the situations that we can observe friction [1]. These manifestations can diverse from a simple walk in the park to grabbing a pen and writing something. Since very early, the human being studied this phenomenon to accomplish a simpler life. A good example is in the ancient times, when it was necessary to build the Giza Pyramids, or the revolutionary invention of the wheel, as shown in the figure

.

This manifestation of contact, nowadays, are studied in real detail in one of many mechanical engineer fields: Tribology.

As said before, the friction between two bodies is a result of contact between both of them. But in fact, it is very connected to the microscopic body saliences, better known as roughness. In this way, we can conclude that even the more polished, machined surface, will undoubtedly have roughness, and hence, will always exist the friction. Therefore, the continuous study of this field of utmost importance, so that friction and wear can be diminished, avoiding less regular material maintenance, in needed situations.

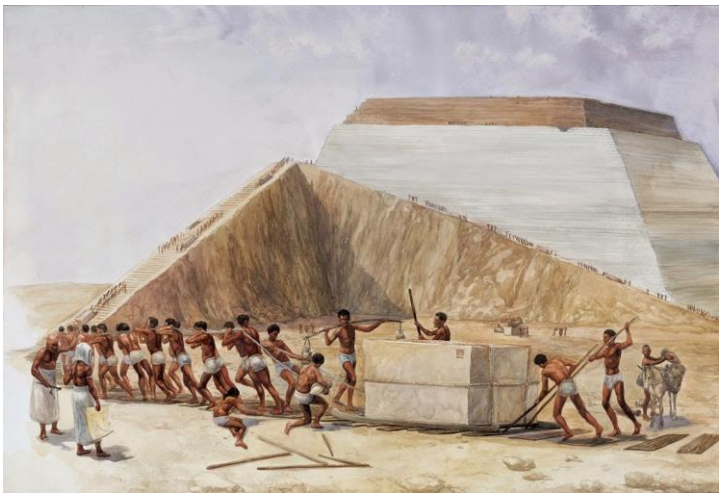

Figure 1-1. Building of the Giza pyramids.

It is of high importance to refer that surface roughness, also know as surface texture, is characterized by series of irregular amplitudes and frequencies that are relevant for the study of the friction, wear and lubrication. These irregularities are seen as peaks and valleys, in a more detailed analysis, and are going to be mentioned in the chapter 2.1.1 [2].

Following the studies of friction, it was Leonardo da Vinci and, two hundred years later, Amontons who, independently, made important statement about this particular theme, and they concluded these two important laws: [2]

1. The friction force is independent from the area of contact between two bodies.
2. The friction force is proportional to the normal force between two bodies.

This second law gave reason to the well known formula, amongst everybody, to calculate the static friction force [3]:

$$F_S = F_N * \mu_S \tag{1.2}$$

Later, in 1780 Later, Coulomb created the third friction law which suggested that the friction coefficient was independent from the velocity of the slip.

In the present, these three laws are still valid and considered correct, and they are used to do primary studies about friction.

1.2. Thesis Structure

This dissertation is divided into 5 different chapters.

The first one, as the same suggests, is connected to a general view of this work.

Chapter 2 is linked to the state of art, where the main theoretical studies are referred and also some important features are mentioned. To end this chapter, a model is presented and explained why it fits good for the investigation.

Third chapter the theoretical analysis is made taking into account the increasing level of complexity. At some point real experimental data are used.

The following chapter is reserved to some experimental tests, if possible.

The last chapter contains the main conclusion about the work done throughout the investigation, and it is also presented some recommendations for any further work.

2. STATE OF ART

This chapter will be divided in some subchapter divided by its importance on this dissertation.

2.1. Tribology

Obviously, over the years, there was an increasing need to model friction, and despite existing a lot of models, only a few are widely known.

In 1929, Tomlinson [4] modeled earth seismic behavior as being an one-dimensional chain of sliding blocks with a given mass, m. Later, Frenkel-Kontorova [5] amongst Tomlinson, were combined to produce the model Frenkel-Kontorova-Tomlinson [6][7] that would change the behavior of the masses by atoms. With this assumption, it was now possible to believe that friction evolved not only major forces, but also atomic forces.

Persson et al. [8] studied friction and slippage, static and dynamic, based on simulations of molecular dynamics.

Since very early, it is known that friction dissipation begin to arise in the exact moment that any tangential force is applied, even though it is not detected by human eye. This is going to be better explained in section “Micro slip”.

It was Greenwood and Williamson who firstly started to model touch on a multi-asperity contact.

Another theoretical model was presented, by Bender et al. [9], to translate the dynamic frictional force depending on the interaction with roughness, taking into account slippage / relaxation phenomena, adhesion and deformation.

2.1.1. Surface texture

When studying friction, wear and lubrication, the definition of topographic deviations is of maximum importance, once it is intimately connected on how loads are transmitted between bodies.

Surfaces are understood as the most external and hardened plans of every solid, and it has fundamental characteristics for this particular subject.

From a general perspective, a surface is normally divided in 4 distinct areas: [2]

1. Material base
2. Deformed layer
3. Oxid layer
4. Bielby layer.

This latter one is produced by melting and surface flow during the machining of the molecular layer. Here, very often, is possible to find a lot of external particles coming from reactions or even from the atmosphere, that affect the contact.

In this dissertation, since it is being dealt with contact between two or more surfaces, it is important to keep in mind that, besides theoretical models and assumptions, there is no surface which can be considered as smooth. For this reason, it is evident that these fluctuations are controlled by the finishing processes by which are produced [2].

For this reason, surface texture is divided in two different subtypes:

1. Macro roughness or waviness, which is caused by the vibration of tools
2. Micro roughness, which is composed by peaks, or asperities, and valleys.

Theoretically, to characterize surface roughness, one of two methodologies can be used:

1. *"Centre-line average roughness value":*

$$R_a = \frac{1}{n}\sum_{i=1}^{n}|z_i| \tag{2.1}$$

In which R_a represents the mean vertical deviation from the centre line.

2. *"Root mean square value":*

$$R_q = \left[\frac{1}{n}\sum_{i=1}^{n}({z_i}^2)\right]^{(\frac{1}{2})} \tag{2.2}$$

Practically, it can be determined by using a styling profilometer.

Therefore, by the reasons exposed above, this so called roughness, frequently, is characterised by periodicity.

It is easily perceptible that only asperities' peaks are submitted to contact, and hence, this abruptly decreases the contact area, when comparing to smooth cases. For this reason, there is caused a high local pressure, same order of magnitude of Vickers Hardness [4][19]. The investigation on this theme is also important for problems related to thermal transport and for lubrication problems.

The main goal of this kind of problems is to have knowledge on how the asperity react when submitted to contact, and so, knowing the deformation when loaded.

Many models use Hertz theory as a beginning to study this familiarity between surfaces, but there are also many models that make assumptions on it.

Archard (1957) [20] assumed that any surface was made out of small asperities covered by even smaller asperities and so on.

In 1966 [21], Greenwood and Williamson concluded that rough surfaces were made of asperities, which followed a Gaussian distribution, and by making a summation between asperity contact, it was possible to predict the total forces. Their model, has been used since then, suffering a lot of small improvements.

Nyak (1971) developed a Longuett-Higgins' approach (1957), known as the most successful model characterizing rough surfaces created in that time. Nyak's model assumes the surface to be a two-dimensional isotropic stochastic process, and from this model derived a lot and important improvements.

More recently, in references [24][25][26][27][28][29], it was demonstrated that the surface tension has an important role in mechanical behaviour at micro and nano scale.

As demonstrated, this topic is intensively studied because an understanding of asperity interaction and substrate deformation is the starting point to improve the already existing frictional models [30].

Many works regarding this fractal size issue concluded corrected and improved models can adequately predict contact forces between different contacts [31].

2.2. The Hertz theory

Once every body has irregularities on its surface, as explained in the previous subchapter" Surface texture", and it is of greatest concern to be aware of peaks' shape.

As the name suggests, Hertz was the first to solve this problem for elastic contact. Then, in 1956, Pater and Johnson extensively studied this subject, and they indicated that this theory could be use to predict the shape and the contact area caused by a normal pressure. Later, Love [14] and Johnson [15] have also studied it [16]

The main assumption of this theory is that this mostly focus on contact between rounded shape objects, and making a meticulous fractal analysis, every asperity can be seen as this shape.

As this theory is going to be continuously used throughout this dissertation, it was decided that it would be helpful to explain the main possible variations of this hypothesis, starting from the simplest to the most complex.

2.2.1. Two dimensional contact

Imagining we have two cylinders, with radius R_1 and R_2 respectively, contacting each other, by compression of both, and due to the known property **elasticity**, the corpse will deform in such way that the contact goes from a straight line to a rectangle, which has a half-width a. Although this can't be considered as true, the error percentage is so small that it can be ignored, making it a flat contact. The deformation in the centre is greater than in the boundaries, and so the distribution of pressure, the primary factor for deformation, has a parabolic similarity:

$$P(x) = P_0\sqrt{\left[1 - (\frac{x}{a})^2\right]} = \frac{2F_N}{\pi\, a}\sqrt{\left[1 - (\frac{x}{a})^2\right]} \tag{2.3}$$

Where x is the position within the width and a can be calculated using:

$$a^2 = \frac{4\, F_N\, R'}{\pi\, E'} \tag{2.4}$$

Whence R' and E' is the equivalent radius and Young Modulus, respectively and are calculated by:

$$\frac{1}{E'} = \frac{(1 - {\nu_1}^2)}{E_1} + \frac{(1 - {\nu_2}^2)}{E_2} \tag{2.5}$$

$$\frac{1}{R'} = \frac{1}{R_1} + \frac{1}{R_2} \tag{2.6}$$

There is a particularity on the last equation concerning the equivalent radius.

The equivalent radius is calculated by adding both inverse radius, when the surfaces are convex. When they are concave, the equivalent radius is a result of a subtraction.

2.2.2. Three dimensional contact

Once not every contact can be considered as this simple, a two dimensional contact, it was necessary to create one equation that could translate three-dimensional contact, which is the most approximated case to reality.

FIGURE 3.13 e mostrar a area de contacto com os eixos (x,z)

If we press two identical spheres against each other, it is evident that these type of contacts produce rounded contact shapes, as circumferential. In this case, the pressure distribution is given by:

$$P(x,z) = P_0\sqrt{\left[1 - (\frac{x}{a})^2 - (\frac{z}{a})^2\right]} = \frac{3F_N}{2\,\pi\,a^2}\sqrt{\left[1 - (\frac{x}{a})^2 - (\frac{z}{a})^2\right]} \tag{2.7}$$

And, since we are dealing with identical spheres, the width is also the contact radius, and it is given by:

$$a = \sqrt[3]{\frac{3\,F_N\,R_a}{8\,E'}} \tag{2.8}$$

If we were dealing with different spheres, the only difference would be in the equation 2.10 we would change R by R', which could be calculated as is it in equation 2.8.

Within this wide range of contact shapes, it is also essential to mention situations where the contact area, instead of being a circumference, is an ellipse. This happens when one rounded shape cylinder and a sphere are submitted to a normal effort.

As seen witnessed in the previous figure, the area is made out of two different components a and b.

For elliptical contact, the pressure can be measured by :

$$p = \frac{3F_N\,L}{2\,\pi\,a\,b}\sqrt{\left[1-(\frac{x}{a})^2-(\frac{z}{b})^2\right]} \tag{2.9}$$

To get the a and b values the procedure is:

$$a = k_a\sqrt[3]{\left[\frac{3F_N}{4\,E'(A+B)}\right]} \tag{2.10}$$

$$b = k_b\sqrt[3]{\left[\frac{3F_N}{4\,E'(A+B)}\right]} \tag{2.11}$$

k_a and k_b are two constants which are intimately connected to body curvatures and on the angle ϕ between the normal planes which contains these curvatures.

To get this values we first need to know:

$$(B-A) = \frac{1}{2}\left[\left(\frac{1}{R_{11}}-\frac{1}{R_{12}}\right)^2+\left(\frac{1}{R_{21}}-\frac{1}{R_{22}}\right)^2+2\left(\frac{1}{R_{11}}-\frac{1}{R_{12}}\right)\left(\frac{1}{R_{21}}-\frac{1}{R_{22}}\right)\cos(\phi)\right]^{1/2} \tag{2.12}$$

$$(A+B) = \frac{1}{2}(\frac{1}{R_{11}}+\frac{1}{R_{12}}+\frac{1}{R_{21}}+\frac{1}{R_{22}}) \tag{2.13}$$

Then we are able to get the quotient between these two equations:

$$\cos(\gamma) = \frac{(B - A)}{(A + B)} \tag{2.14}$$

Finally we get to know the relation between this constants and k_a and k_b by using the figure below figure 3.15 pg58.

This assessment was made for a contact between rounded cylinder and a sphere, but if we had a straight contacting a sphere, the difference would not be substantial.

Instead of having numerous radius in equation 2.14 and 2.15, we would have less [2].

2.3. Response to loading

There are at least 4 different ways of loading an object: Constant load, Force applied by impact, oscillating tangential and a vibration method.

Rewriting some of what was already been said, for small tangential forces, the displacements are practically elastics, and the compliance of the two bodies is given exactly by the elastic theory. It was Rankin, in 1926, who found the linear and elastic relationship between tangential forces and displacements [12]. But when the tangential force reaches to a certain value, the process differs in a manner that the displacement is not-elastic and there is actually slipping. One thing that was not mentioned before, was that, when there is the appliance of tangential forces, fretting takes place over an annular area around and spreads inwards with the increasing tangential force. Under larger forces, the asperities will, however, deform plastically. Rabinowicz (1951) deduced that, before the static friction ratio started to decrease, microscopic displacements occurred.

When applying oscillating tangential forces, which the maximum value is lower than the necessary to cause slip, was found that the displacement would alternate with the applied force, and the relationship between force and displacement is plotted as hysteresis loop.

2.4. Micro slip

The contact reaction, between two bodies, when submitted to a shear force, F_T, was firstly described by the already mentioned Amontons-Coulomb's law. These scientists concluded that, below the nominal static threshold, F_{ns}, no apparent displacement would occur and also that a dynamic friction coefficient would define the contact when sliding would take place.

However, as mentioned before, the onset of friction dissipation starts for shear forces lower than nominal static threshold, F_{ns},. This is a prime importance topic in mechanical engineering, because although there is no major displacement, fretting and wear are in constant action. For this reason, micro slip must be taking place.

Mindlin et al. [11]and later Johnson [12][13]were who firstly studied this issue.

Goodman & Brownin (1962) proved that the responses of displacements of hertzian macroscopic contacts subject to a tangential force of less amplitude than F_{ns}, would demonstrate a hysteresis loop due to an interfacial dissipative process.

To account this losses, Mindlin et al. had proposed a micro-slip model, which assumed what has been said before: within the contact zone, there is no major slip, and the tangential and normal force should follow this law $F_T < F_N * \mu$. Whenever this two forces are equal, the stress satisfies Coulomb's friction law.

Hereupon, it is possible to conclude that the friction ratio is not constant during the contact.

2.5. Theoretical model used

This model comes from on of the greatest tribology thinkers, the well known Mindlin. In reference [12], Johnson used a model that could translate, as the name implies, the surface interaction between elastically loaded bodies under tangential forces.

In an unlubricated environment, those experiences involved a hard steel ball and a hard still flat. The elements put into contact were the main reason why it was decided to use this model. In many real contact cases, if one element has a much bigger radius comparing to the other, it can be considered as flat, whilst every asperity (surface in contact) can be considered as rounded shape. The results obtained were important because they gave support to Mindlin's theoretical elastic analysis.

At this moment, it is reasonable to declare that when two bodies are pressed against each other, and also submitted to a tangential force, they will only have micro-displacements until that tangential force, F_T, exceeds the critical value, $F_N * \mu_S$. Thereafter, major sliding will occur.

This model was based on incipient theoretical work of Mindlin (1949), and also Mindling, Mason, Osmer & Deresiewicz (1952)

In the first, Mindlin studied two elastic spheres under normal pressure and tangential force, over a circumferential of radius a, which was proportional to ${F_N}^{1/3}$ and the pressure distribution according to Hertz theory, analyzed in the chapter 2.2. When adding the tangential force, the displacement, from one body to another, arise, and every point in both bodies have the same displacement.

This first embryonic study, by Mindlin, concluded that the displacement, until slip, could be translated by:

$$x = \frac{(2 - \upsilon)}{4\,C\,a} \,.\, F_T \tag{2.15}$$

In which υ represents the Poisson's ratio and C the Modulus of rigidity.

This model is practically in the final form and, such as, Mindlin assumed that

the shear traction could not exceed the product between $p * \mu_S$. To satisfy this, only within the contact area are assumed to have relative slip between both bodies, and none besides the contact radius.

So, the modified model happens to be:

$$x = \frac{2 - v}{4\ C\ a}\ .F_N * \mu_S \left[1 - (1 - \frac{F_T}{F_N * \mu_S})\right]^{2/3} \tag{2.16}$$

The contact radius, a, also referred as contact half-width, between a sphere and a plane, could be calculated using the following equation:

$$a = 1{,}11 \sqrt[3]{\frac{F_N\ R_{asp}}{E'}} \tag{2.17}$$

Since the main goal of this investigation is to get a knowledge on the friction coefficient through the contact, the equation 2-16 must be in order of F_T.

$$F_T = \left[1 - \left(1 - \frac{8\ \Delta x\ a\ C}{3\ (2 - v)\ \mu\ F_N}\right)^{\frac{3}{2}}\right] \mu\ F_N \tag{2.18}$$

3. CONTACT STUDY

3.1. Theoretical study

Along this chapter, it will be presented some theoretical approaches to many different assessments, which will be divided into distinct subchapters.

When two bodies are put into contact, there are two different ways to examine these situations. It can be done either macroscopically or microscopically. This last, when the contact is observed very closely, there will always be a discrete number asperities touching each other, and this gave rise to the rough surface methodology already explained. As referred many times, one surface can only be considered as smooth in a theoretical point of view, but in this research it will also be studied, to have a better understanding on how this second affects the contact.

The main goal of this work is to do an evaluation on different contacts, getting knowledge on how does the friction coefficient improves over the contact and comparing it to Kalker's theory, which consists in plotting this coefficient in terms of velocity ratio. This quotient will get to a point that becomes constant, and in that moment we are dealing with changes along the contact: It went from rolling to sliding.

It is also required to know the maximum displacement.

To have a better data changing layout, the obtained values were plotted into a graphic so that the differences could be easily noticed.

The disposition of this chapter is made in chronological order, according to the assessments done.

3.1.1. Normal Static Contact

The first approach done was obviously the simplest, where the bodies were only submitted to one effort, which in this case was a normal force. For this reason, this primary evaluation was made in the most basic contact conditions possible, once the was neither rolling nor sliding between both subjects.

3.1.1.1. Sphere and a flat plan

As a continuation of this chapter's title, here the analysis is represented by a sphere pressed against a flat plane, without existence of any other effort.

The main purpose of this initial step is to get a general view on how does the stiffness, represented as k, would be affected by the changing parameter.

In figure AP 3-1, the main data related to contact objects are revealed, and it is important to mention that no specific article nor experimental data linked to any real investigation were used. These data were used randomly, merely to do this assessment, so it was possible to have a general knowledge on how it would affect the contact.

This can be calculated using its relationship with the normal force and according to [2], where it is possible to find the previous steps which conducted to the expressions used in further work.

From a contact between a sphere and a plane it ensued that the mass centre had such displacement, named as δ, given by:

$$\delta = \left(\frac{9{F_N}^2}{16\, E'^2\, R} \right)^{1/3} \tag{3.1}$$

As expected, the displacement has an intimate relationship with the effort submitted.

The predicted area between a sphere and a plane is a circle, and for this reason the area is calculated by its expression:

$$A = \pi a^2 = \pi R \delta \tag{3.2}$$

As specified, besides the estimation, the values are also plotted.

In the first approach, only the Young's modulus, normal effort and sphere radius were modified as observed in the figures below. These figures only show the plotting, as the data is shown from Figure AP 0-1 to Figure AP 0-3, for Figure 3-1, Figure 3-2 and Figure 3-3, respectively.

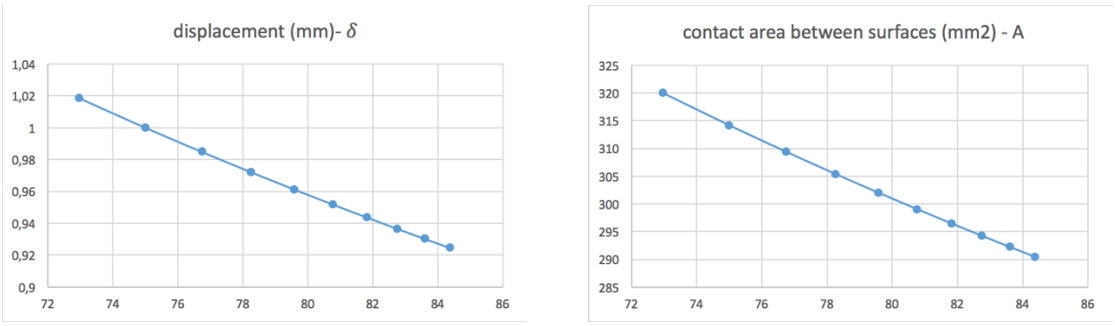

(a) (b)

Figure 3-1. (a) Displacement due to E_1 increments; (b) contact area due to E_1 increments.

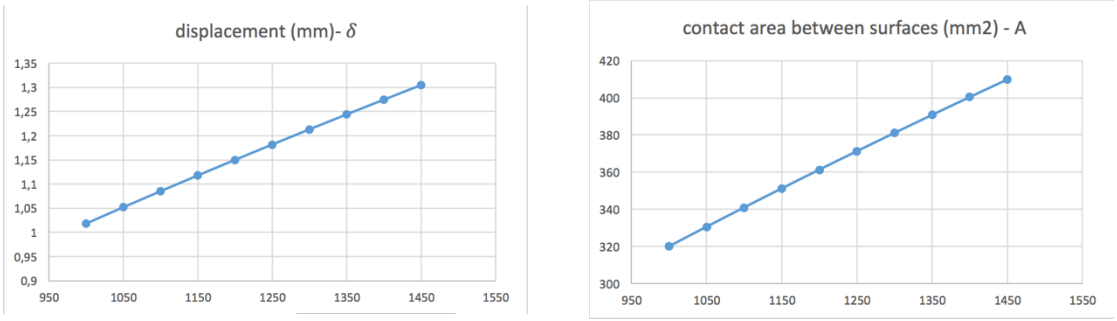

(a) (b)

Figure 3-2. (a) Displacement due to load increments; (b) contact area due to load increments.

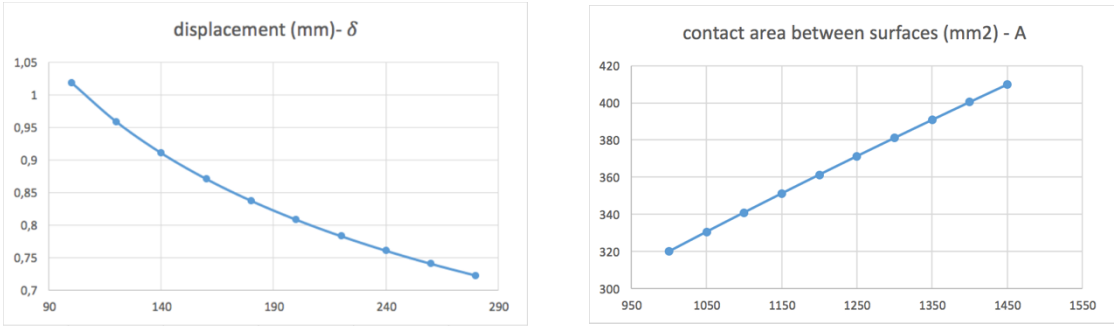

(a) (b)

Figure 3-3. (a) Displacement due to radius increments; (b) contact area due to radius increments.

Besides the third point, first both analysis have linear dependence on modifications.

In this last assessment of this first step, stiffness is going to be analysed, and it is no more difficult than the previous approach, but is important to know how to calculate it.

Stiffness comes from the relationship between the normal force and the displacement:

$$k_i = \frac{dF_N}{d\delta} = \frac{d(\frac{4}{3}E_i{'}R_i{}^{1/2}\delta_i{}^{3/2})}{d\delta_i} = \frac{3}{2}\left[\frac{4}{3}R_i{}'^{1/2}\ E'\delta_i{}^{1/2}\right] \tag{3.3}$$

At this point, it is going be done different stiffness analysis based on the data obtained. Therefore, besides the stiffness assessment on improving data, it will be also added the particularity of increasing number of contact points, for an increasing smaller radius, assuming this as the first approach to roughness existence.

Thus, it all began with the assessment related to radius improvement. After this, as mentioned, for the second assessment, it was decided to decrease the radius size in a inversed proportion as the number of contacting points increased, in other words $R_i = \frac{R_1}{n_i}$, in which R_1 is the initial radius (100 mm) and n_i is the number of contacting points.

Similar to the latter evaluation, the data will also be plotted into a graphic to a better understanding, as shown Figure 3-4 .

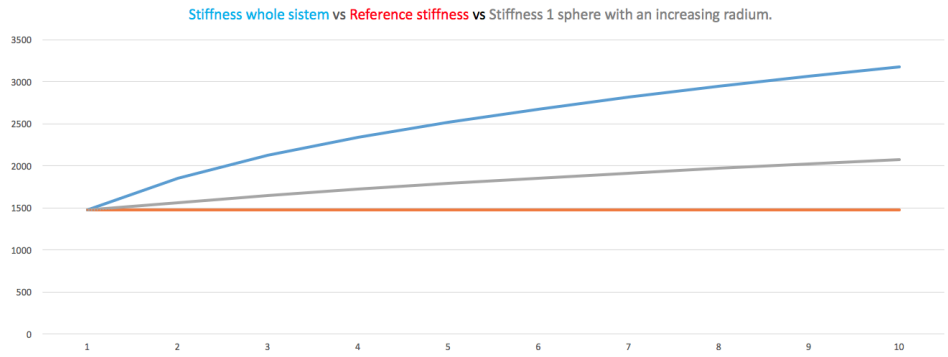

Figure 3-4. Stiffness graphic evaluation related to Figure AP 0-5 data.

In this graphic shown above, all three plotting are according to the title's colours.

For this beginning, it is now intelligible why it was decided to study the contact between a sphere and plane and not the contact between any other geometric shape: Due to its intimate connection with roughness.

3.1.2. Normal and tangential load along the contact

3.1.2.1. Smooth stationary rolling

At a more advanced stage, it is now time to add other force's components, in order to make this theoretical study as more realistic as possible. In this initial approach, two cylinders were submitted to contact, and besides the normal force applied, tangential forces were added, not directly but by a relative motion between bodies, generated by a rolling velocity appliance. See figure to a better understanding.

Two bodies are said to be rolling when they have different angular velocities [17], $w_1 \neq w_2$, and for this reason, the *angular velocity of roll* is then the difference between both:

$$\Delta w = |w_1 - w_2| \tag{3.4}$$

Furthermore, if there is any difference between linear velocities, V, it will also exist, apart from the angular velocity of roll, a *sliding velocity*. This component is expressed in the same way as the latest, having only this particular change: $V = wR$

$$\Delta V = |w_1 R_1 - w_2 R_2| = |V_1 - V_2| \tag{3.5}$$

The term *rolling velocity*, $\bar{V}$, should be carefully defined, as it is different from *sliding velocity* or *angular velocity of roll*. This must be taken into account especially if the contact point/area between both surfaces is not at rest. In other words, if one or both centre of the cylinders is in linear motion.

However, if the bodies are rotating about fixed centres then the rolling velocity is [17]:

$$V_r = \frac{1}{2}|V_1 + V_2| = \tag{3.6}$$

Studying the situation shown in the figure, it can be considered as a stationary rolling between cylinder and plane.

This issue was first studied by Carter [15][18], where he predicted that the tangential effort would be limited by Coulomb's law and that the pressure, unaffected by friction, would get an elliptical distribution, quoting Hertzian theory.

Carter noticed, for low sliding velocities, the existence of a friction coefficient that would nullify the slide and also the presence of tangential forces less than the limit assumed by Coulomb. Figure artigo frances adaptada

Combining this information, the tangential effort results from a sliding rate, $\bar{\xi}$, which is defined by a quotient between the sliding velocity (equation 3.5) and rolling velocity (equation 3.6) and these properties are connected by the following equations:

$$\bar{\xi}(\%) = \frac{\Delta V}{V_r} \tag{3.7}$$

$$\frac{F_T}{\mu F_N} = 1 - (1 - \overline{|\xi|})^2 \tag{3.8}$$

This was the principle used to this second approach to mechanical contact between solids.

From now on, the procedure will be demonstrated also, as last approach, using random values.

From a theoretical point of view, it is already explained in the chapter2.. that the tangential force could not be bigger than the product between μF_N, and so the maximum value admissible for it quotient 1. When this value is reached, if the same contact conditions are still taking place, it is being faced a saturated contact in which no more rolling is possible. Contrary of what is shown in Figure 3-5, the evolution does not decrease but remains constant, as displayed in Figure 3-6.

ε Increments	ε=(△V / Vr)	(Ft/μFn)=(1-(1-ε)^2)
0,07	0	0
0,04	0,07	0,1351
0,03	0,14	0,2604
0,01	0,21	0,3759
	0,28	0,4816
	0,35	0,5775
	0,42	0,6636
	0,49	0,7399
	0,56	0,8064
	0,6	0,84
	0,64	0,8704
	0,68	0,8976
	0,72	0,9216
	0,76	0,9424
	0,8	0,96
	0,84	0,9744
	0,87	0,9831
	0,9	0,99
	0,93	0,9951
	0,96	0,9984
	0,97	0,9991
	0,98	0,9996
	0,99	0,9999
	1	1
	1,07	0,9951
	1,14	0,9804
	1,21	0,9559
	1,28	0,9216
	1,35	0,8775

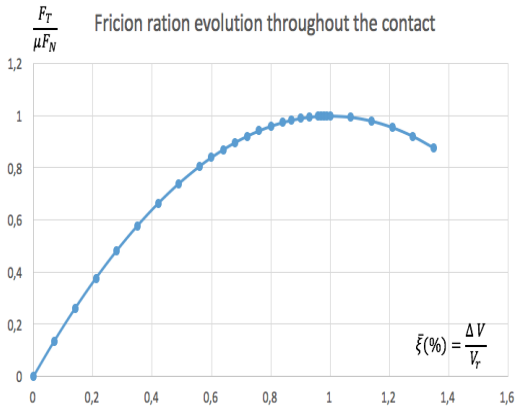

(a) (b)

Figure 3-5. (a) Effort ratio calculation without any $\bar{\xi}$>1 condition; (b) Plotting the data into a graphic.

ε Increments	ε=(△V / Vr)	(Ft/μFn)=(1-(1-ε)^2)
0,07	0	0
0,04	0,07	0,1351
0,03	0,14	0,2604
0,01	0,21	0,3759
	0,28	0,4816
	0,35	0,5775
	0,42	0,6636
	0,49	0,7399
	0,56	0,8064
	0,6	0,84
	0,64	0,8704
	0,68	0,8976
	0,72	0,9216
	0,76	0,9424
	0,8	0,96
	0,84	0,9744
	0,87	0,9831
	0,9	0,99
	0,93	0,9951
	0,96	0,9984
	0,97	0,9991
	0,98	0,9996
	0,99	0,9999
	1	1
	1,07	1
	1,14	1
	1,21	1
	1,28	1
	1,35	1

(a)

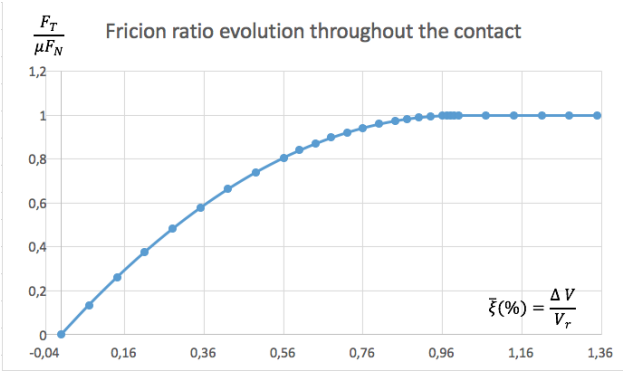

(b)

Figure 3-6. (a) Parameter calculation with $\bar{\xi}$>1 condition; (b) Plotting the data into the correct graphic.

3.1.2.2. Rough stationary rolling

3.1.2.2.1. Rectangular contact shape

In this second subchapter related to stationary rolling, the problem at issue is same as the latest but regarding a microscopic analysis, hence, a rough analysis.

As suggested previously, asperities are considered as rounded shapes, and as expected, the biggest difference is that the contact is made out of numerous points. These points are considered to be equally distributed, using a periodicity, p. This distance has commonly the same value which is p= 0,05 mm.

For this new approach, the methodology is quite similar to the previous one. First of all, besides knowing the main data, it is a must to know the number of contact points through the contact, and to calculate this parameter, the width length and periodicity should be taken into account:

- Number of asperities over the length:

$$nº\ asperites = \frac{L}{p} \tag{3.9}$$

- Number of asperities over the width:

$$nº\ asperites = \frac{a}{p} \tag{3.10}$$

Similarly to the first approach to rough contact, in the subchapter 3.1.1.1, the Normal Force is going to be divided by each asperity, not equally, but through a intimate relationship with normal pressure, as Hertzian theory suggests.

On the figure below, main data will be shown, but now it would be of high interest to have it closer to real data. To succeed in this, $P_0 = \frac{2\,F_N}{\pi\,a}$ should be around 1-2 GPa.

It is of major importance to notify the fact that from figure 3-13 to 3.1 disposed in this section is related to the data shown in Figure AP 0-6

Using equation 2.3, it is possible to plot pressure distribution, as shown in the figure below

P(x)
0
289,3785248
721,8775671
921,483961
1033,35199
1084,969197
1091,24969
1084,969197
1033,35199
921,483961
721,8775671
289,3785248
0

(a)

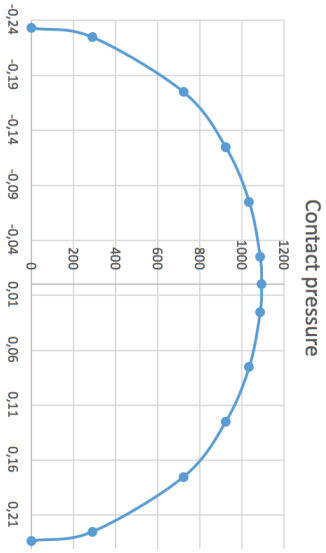

(b)

Figure 3-7. (a) Contact pressure distribution between two cylinders, rectangular shape (b) Plotting the data into a graphic.

It is of high interest to know that points without filling colours, in Figure 3-7 (a), are not considered asperities, but valleys.

It is from this moment that this assessment differs from the lattest.

Due to this arc-shape pressure distribution, it is noticeable that, throughout the width, the normal force is not constant. To get this important parameter it could be calculated either using the integral or calculating rectangular areas under the graphic, in which the rectangular width middle point was the asperity. The second choice was preferred, once for the next step, the circular contact shape, it would be more difficult to calculate by the first choice. The error rate is not that significant, and so it is acceptable to calculate the areas.

The figure below, shows how the pressure is related to the contact.

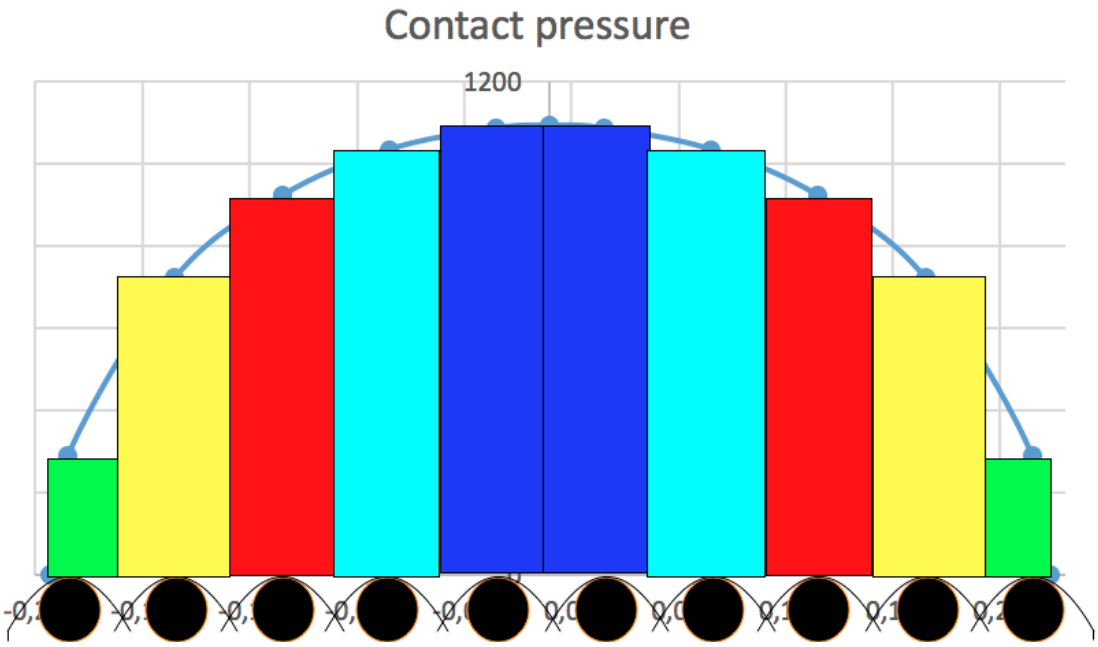

Figure 3-8. Contact normal force, cylinder-cylinder.

By doing this step, normal force on each column, along the contact, is discovered, and so, since it is wanted to study the contact for one asperity, then this value should be divided by the number of asperities through the length. This division is done due to contact shape. As the contact shape is rectangular, it is known that in the same column, the normal force does not suffer any change. At this stage, points which are not considered as asperities are not taken into consideration.

Let the Table AP 0.2 gives a better general view on the results.

Having knowledge on this distribution, it is now possible to analyse each asperity behaviour.

Now, it is the moment that the model proposed is used, equation 2-18.

Besides calculating the, already known, normal force, it is also required to calculate the asperity half width, a, width and the displacement between both asperities, x.

For the first barrier, equation 2-17 is used to calculate the contact through every asperity width, using the normal force calculated in the last step.

In the table disposed here below, the asperity width value for each position are shown.

Table 3.1. Calculation of asperity width based on F_N for each asperity.

	JOHNSON ARTICLE
Fn(per asperity)	Asperity width - a(i)
0	0
0,048260225	0,001464804
0,180469392	0,002273619
0,23037099	0,002466375
0,258337998	0,002562394
0,271242299	0,002604368
0,271242299	0,002604368
0,258337998	0,002562394
0,23037099	0,002466375
0,180469392	0,002273619
0,048260225	0,001464804
0	0

For the second task, it is a more complicated issue. This required displacement is not so evident as it seems, because this displacement is related to each asperity and not the body as a whole.

At this point, rolling and sliding velocities are then used, and both are intimately connected, as known as SR, or also commonly referred as slide-to-roll ratio.

First of all, the contact between two asperities is characterized by a middle point, if both asperities' centres of mass are not vertically positioned. This middle point was assumed to be the position in which the contact was made in the previous calculation. So, for this reason, each middle point is equally far of both neighbours, by its periodicity. Then the rolling velocity, which was told to be the mean velocity between both bodies, is used,

together with the distance covered through the contact, to find out how long did it take to reach the required middle point.

This step is done by using the normal equation for velocities:

$$\Delta t = \frac{\Delta x}{V_r} \tag{3.11}$$

Table 3.2. Time to get to the theoretical asperity position.

Δ xi	Δ t1 (s)
distance covered on width (mm)	**time to get to asperity (s)**
0,008354393	2,17019E-05
0,058354393	0,000151585
0,108354393	0,000281468
0,158354393	0,000411351
0,208354393	0,000541234
0,258354393	0,000671117
0,308354393	0,000801001
0,358354393	0,000930884
0,408354393	0,001060767
0,458354393	0,00119065

Knowing this period of time, it is possible to calculate the displacement for asperities in both bodies, by using the same relationship as in equation 3.11:

$$x_i = V_i \ \Delta t \tag{3.12}$$

Then, finally, is possible to calculate the displacement between asperities, by subtracting both displacements, as shown in Table 3.3.

Having all required parameter deducted, it is possible to calculate the tangential force on contact, by using the model proposed in equation 2.18 .

Since these calculations were made in Excel, and not using any program, there were made some variable changes, and to make this it easier, the calculation was made into different steps:

1. $B = \frac{8\ x\ a\ C}{3\ (2-\upsilon)\ \mu\ F_N}$
2. $Y = (1 - B)^{\frac{3}{2}}$
3. $F_T = (1 - Y)\ \mu\ F_N$

These different steps were used not only for the facilities, but also to stress the importance that the variable B can not be bigger than 1, due to second step. For this, B calculation was divided in two conditions:

1. If $B < 1$, then:

$$B = \frac{8\ x\ a\ C}{3\ (2-\upsilon)\ \mu\ F_N}$$

2. If $B \geq 1$, then it assumes it major value, linked with slipping movement:

$$B = 1$$

Table 3.3. Calculation of F_T on each asperity based on the data calculated previously.

IF B < 1	IF B > 1		Per asperity position
B	B	Y= (1-B)^(3/2)	Ft= (1-Y)*Fn
0,021028435	1	0,968623756	0,000454267
0,060966249	1	0,909958955	0,004874896
0,096201007	1	0,859226731	0,009729023
0,130253542	1	0,811127271	0,014637901
0,165901127	1	0,761774273	0,019385068
0,205713373	1	0,707890161	0,023769763
0,253635224	1	0,644802485	0,027528304
0,318160182	1	0,563019633	0,03020028
0,426631726	1	0,434160679	0,030635003
1,153701494	1	0	0,014478067
	0	0	0

Since the main goal is to plot F_T evolution along the contact it is necessary to get the overall F_T. This process, comparing to what was done with the normal force before, is the opposite. It is now required to multiply the tangential effort by the number of asperities in each column and then summing them all. This procedure is shown in the Table AP 0.4

After getting the parameter required, it is possible to draw the graphic with the variables $\left(\frac{F_T}{\mu F_N}, \bar{\xi} = \frac{\Delta V}{V_r}\right)$. When changing the angular velocity for cylinder number two it will also change the sliding rate, which is directly connected with the displacement between both bodies centre of mass, which in turn will lead to a new ration between F_T and μF_N, and so on.

For this data exposure, the sliding rate shown in Table AP 0.4 was selected in purpose so that it would be possible to display both situations: rolling and sliding, clearly identified. In the end, it will be get to a point in which every asperity is sliding and the F_T will not change, as disposed in the table below.

Table 3.4 Situation in which every asperity is in sliding condition.

IF B < 1	IF B > 1		Per asperity	Per column
B	B	Y= (1-B)^(3/2)	F_T= (1-Y)*uFn	F_T
	0	0	0	
1,05670529	1	0	0,014478067	2,895613499
3,063630582	1	0	0,054140818	10,82816351
4,834221447	1	0	0,069111297	13,82225942
6,545404135	1	0	0,077501399	15,50027986
8,336740056	1	0	0,08137269	16,27453796
10,33735543	1	0	0,08137269	16,27453796
12,74548865	1	0	0,077501399	15,50027986
15,98794884	1	0	0,069111297	13,82225942
21,43878022	1	0	0,054140818	10,82816351
57,97494944	1	0	0,014478067	2,895613499
	0	0	0	0
			Total F_T=	118,6417085

After changing the sliding rate several times, it was finally possible to plot the graphic was wanted, so it could be compared with the Kalker's linear theory.

The sliding rates and ratio between forces are shown in the following table.

Table 3.5 Relationship between sliding rate and .

ΔV/Vr (%)	$\sum F_T$	$\sum F_T$ / (Fn . μ)
0,001000005	1,971296798	0,016427473
0,003000045	5,857575833	0,048813132
0,00600018	11,54086694	0,096173891
0,009000405	17,0382245	0,141985204
0,0100005	18,8267108	0,156889257
0,011000605	20,59197134	0,171599761
0,01200072	22,3330415	0,186108679
0,015001125	27,39701154	0,22830843
0,01600128	29,02393741	0,241866145
0,01800162	32,13846618	0,267820552
0,020002	35,13851482	0,292820957
0,02200242	38,08474851	0,317372904
0,025003125	42,40017239	0,35333477
0,030004501	49,30201204	0,4108501
0,035006126	55,81342027	0,465111836
0,040008002	61,88974693	0,515747891
0,045010127	67,44867792	0,562072316
0,050012503	72,28350396	0,602362533
0,055015129	76,7097873	0,639248228
0,060018005	80,75799267	0,672983272
0,070024509	87,40342097	0,728361841
0,075028136	90,28398616	0,752366551
0,080032013	92,78742752	0,773228563
0,08503614	94,98237564	0,791519797
0,090040518	97,01805074	0,808483756
0,100050025	100,4086122	0,836738435
0,150112584	109,9878085	0,916565071
0,2002002	113,8665755	0,948888129
0,250312891	115,5524734	0,962937278
0,300450676	116,7308675	0,972757229
0,350613574	117,186857	0,976557142
0,501253133	117,6958954	0,980799128
0,601805416	117,9922678	0,983268898
0,803212851	118,4583618	0,987153015
0,904068307	118,6056548	0,988380457
0,955637501	118,6417085	0,988680904
1,005025126	118,641708497898	0,988680904
2,02020202	118,641708497898	0,988680904

And plotting this data, this graphic is obtained:

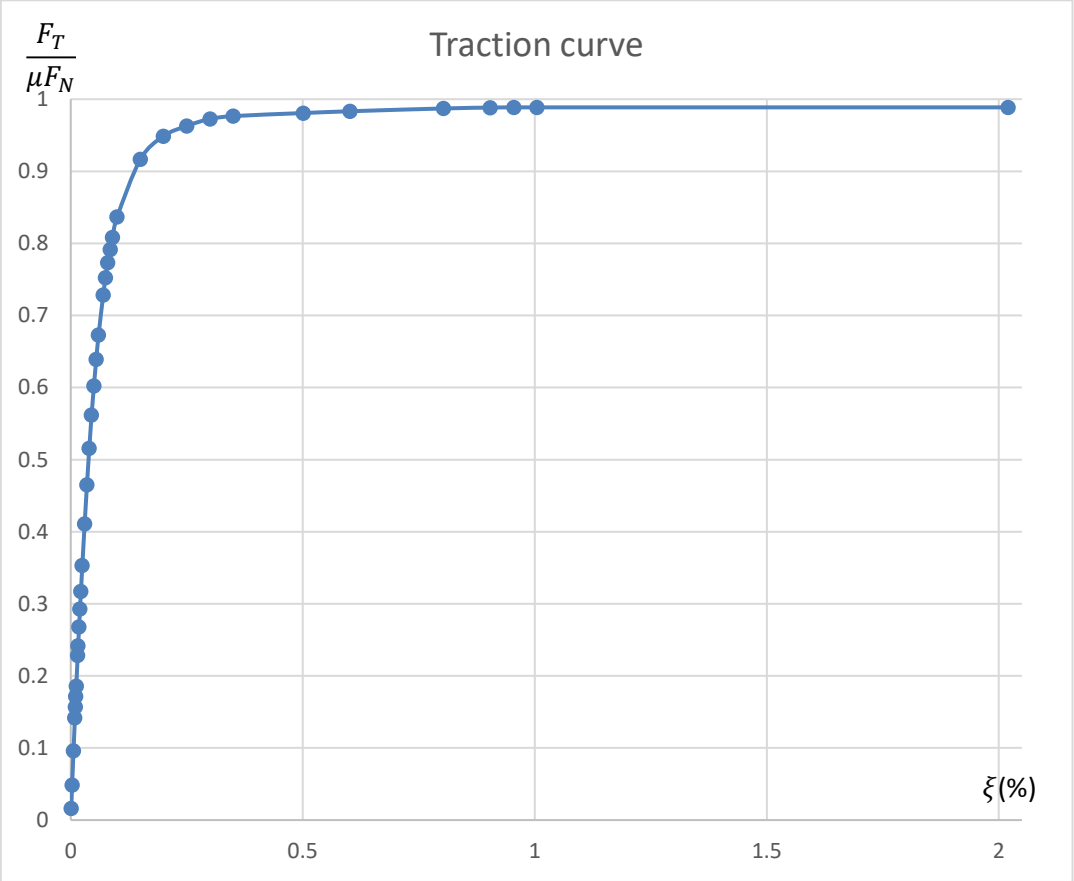

Figure 3-9. Relationship between SR and effort ratio, for rectangular contact shape.

3.1.2.2.2. Circular contact shape

For this next, and final, step, the approach is almost identical. But first, some assumptions were made so that the assessment would become easier.

Similarly to a rectangular contact shape, this one has also some symmetric relations regarding the efforts and subsequent actions. As the procedure advances, these assumptions will be explained together with a figure, for a better understanding.

As explained, the contact between two cylinders can generate a circular contact shape, depending on how their axes are disposed, however, as mentioned before, this chapter was reserved to real experiences data analysis. For this reason, some calculation are avoided as it is part of initial data given, such as normal force, maximum contact pressure, and both contact widths. This information is disposed in Table AP 0.5.

Since the contact area is a circle, then, regarding the asperities' position, they are symmetric referring to both axes, and this makes the pressure also symmetric, as seen in the figures disposed previously.

On Figure AP 0-7 and Figure AP 0-8 it is possible to find this asperity distribution.

Due to its symmetric properties, it could be only analysed one quarter, but it would not be correct, and so the circle's upper half of the will be all analysed. This "mistake" is going to be stated later.

Having the pressure distribution displayed, on Figure AP 0-9, it is now time to get the normal force on each asperity. The procedure is the same, but as noticed in Figure AP 0-7, there are some highlighted asperities. This is related to the fact that these asperities are critical due to their area, once they are closer to the contact boundary. The differentiated point represents the point of symmetry inside the same quarter. For these, the area was specifically calculated, while the others area is p^2.

This step requested the calculation of the integral of the circle equation.

$$\int_{v_i}^{v_{i+1}} \sqrt{a^2 - x^2} = \left[2a \sin^{-1}(\frac{5x}{2}) + \frac{x}{2}\sqrt{a^2 - x^2}\right]_{v_i}^{v_{i+1}} \quad (3.14)$$

In which v_i and v_{i+1} represents the x values for the valleys (known to be the area extremities).

This integral, as all, gives the area below the graphic, therefore, it is needed to subtract the area already known by the relation p^2. Let the figures give a better explanation.

Table 3.6 Relationship between sliding rate and .

Area of critical asperities								
Asperity	**x1**	**x2**	**INTEGRATION**		**RESULT**	**-**	**KNOWN AREA**	**CRITICAL AREA**
1	0	0,05	0	0,019947794	0,019947794	-	0,0175	0,002447794
2	0,05	0,1	0,019947794	0,039579337	0,019631543	-	0,0175	0,002131543
3	0,1	0,15	0,039579337	0,058562486	0,018983149	-	0,0175	0,001483149
4	0,15	0,2	0,058562486	0,076528918	0,017966432	-	0,015	0,002966432
5	0,2	0,25	0,076528918	0,09304176	0,016512842	-	0,015	0,001512842
6	0,25	0,3	0,09304176	0,107531236	0,014489476	-	0,0125	0,001989476

Asperity are counted clockwise.

Continuing, it will be possible to get the normal force for each asperity.

NORMAL LOAD FOR HALF																	
			0	0	0	0	0	0	0	0	0	0					
		0	0	0	0,46	1,27	1,70		1,70	1,27	0,46	0	0				
340,1416756		0	0,47	2,32	2,50	2,80	2,94		2,94	2,80	2,50	2,32	0,47	0			
	0	0,94	2,33	2,94	3,33	3,56	3,67		3,67	3,56	3,33	2,94	2,33	0,94	0		
	0,47	2,33	3,07	3,56	3,88	4,09	4,18		4,18	4,09	3,88	3,56	3,07	2,33	0,47		
0	2,32	2,94	3,56	3,99	4,28	4,46	4,55		4,55	4,46	4,28	3,99	3,56	2,94	2,32	0	
0,46	2,50	3,33	3,88	4,28	4,55	4,72	4,81		4,81	4,72	4,55	4,28	3,88	3,33	2,50	0,46	
1,27	2,80	3,56	4,09	4,46	4,72	4,89	4,97		4,97	4,89	4,72	4,46	4,09	3,56	2,80	1,27	
1,70	2,94	3,67	4,18	4,55	4,81	4,97	5,05		5,05	4,97	4,81	4,55	4,18	3,67	2,94	1,70	

Figure 3-10. Normal load by half of the contact.

As seen, the normal load distribution is in agreement with the force primarily applied.

Not changing what has been done, now it is needed to get the tangential force value, by doing the same data validation. Once the procedure is equal, only the final results will be shown:

1. At first, getting the half-width asperity.

					0	0	0	0	0	0	0						
			0	0	0,03447077	0,04830581	0,05326918		0,05326918	0,04830581	0,03447077	0	0				
		0	0,03469929	0,05907535	0,06054470	0,06290618	0,06393823		0,06393823	0,06290618	0,06054470	0,05907535	0,03469929	0			
	0	0,04378229	0,05916659	0,06393823	0,06661566	0,06814060	0,06884330		0,06884330	0,06814060	0,06661566	0,06393823	0,05916659	0,04378229	0		
0	0,03469929	0,05916659	0,06489315	0,06814060	0,07014974	0,07134478	0,07190666		0,07190666	0,07134478	0,07014974	0,06814060	0,06489315	0,05916659	0,03469929	0	
0	0,05907535	0,06393823	0,06814060	0,07075988	0,07244740	0,07347198	0,07395861		0,07395861	0,07347198	0,07244740	0,07075988	0,06814060	0,06393823	0,05907535	0	
0,03447077	0,06054470	0,06661566	0,07014974	0,07244740	0,07395861	0,07488642	0,07532958		0,07532958	0,07488642	0,07395861	0,07244740	0,07014974	0,06661566	0,06054470	0,03447077	
0,04830581	0,06290618	0,06814060	0,07134478	0,07347198	0,07488642	0,07576007	0,07617867		0,07617867	0,07576007	0,07488642	0,07347198	0,07134478	0,06814060	0,06290618	0,04830581	
0,05326918	0,06393823	0,06884330	0,07190666	0,07395861	0,07532958	0,07617867	0,07658608		0,07658608	0,07617867	0,07532958	0,07395861	0,07190666	0,06884330	0,06393823	0,05326918	

Figure 3-11. Asperity half-width on circular contact.

2. Then, calculating the displacement between asperities centres of mass.

Here it is understood why this assessment should be done by half and not by quarters.

					0	0	0	0	0	0	0						
			0	0	0,00000014	0,00000064	0,00000114		0,00000164	0,00000214	0,00000264	0	0				
		0	0,00000008	0,00000058	0,00000108	0,00000158	0,00000208		0,00000258	0,00000308	0,00000358	0,00000408	0,00000458	0			
	0	0,00000015	0,00000065	0,00000115	0,00000165	0,00000215	0,00000265		0,00000315	0,00000365	0,00000415	0,00000465	0,00000515	0,00000565	0		
0	0,00000006	0,00000056	0,00000106	0,00000156	0,00000206	0,00000256	0,00000306		0,00000356	0,00000406	0,00000456	0,00000506	0,00000556	0,00000606	0,00000656	0	
0	0,00000035	0,00000085	0,00000135	0,00000185	0,00000235	0,00000285	0,00000335		0,00000385	0,00000435	0,00000485	0,00000535	0,00000585	0,00000635	0,00000685	0	
0,00000005	0,00000055	0,00000105	0,00000155	0,00000205	0,00000255	0,00000305	0,00000355		0,00000405	0,00000455	0,00000505	0,00000555	0,00000605	0,00000655	0,00000705	0,00000755	
0,00000018	0,00000068	0,00000118	0,00000168	0,00000218	0,00000268	0,00000318	0,00000368		0,00000418	0,00000468	0,00000518	0,00000568	0,00000618	0,00000668	0,00000718	0,00000768	
0,00000024	0,00000074	0,00000124	0,00000174	0,00000224	0,00000274	0,00000324	0,00000374		0,00000424	0,00000474	0,00000524	0,00000574	0,00000624	0,00000674	0,00000724	0,00000774	

Figure 3-12. Displacement between asperities.

As noticed, the displacement between asperities is obviously not symmetric referring z-axes, and that is the main reason it was decided to do this assessment this way.

3. Calculation of the parameter B, having the same conditions, as previous assessment:

IF B < 1 , THEN B=

					0	0	0	0	0	0	0						
			0	0	0,00405333	0,00933474	0,01365518		0,01963412	0,03114689	0,07544439	0	0				
		0	0,00230651	0,00565719	0,01001425	0,01356385	0,01727957		0,02142963	0,02642591	0,03315586	0,03968714	0,12912343	0			
	0	0,00273908	0,00634629	0,00958447	0,01265267	0,01574666	0,01900659		0,02258633	0,02670854	0,03176851	0,03863490	0,04996426	0,10009709	0		
0	0,00161168	0,00540077	0,00851846	0,01137982	0,01418495	0,01704686	0,02006273		0,02334397	0,02704623	0,03142323	0,03695755	0,04477786	0,05871161	0,18479167		
0	0,00337260	0,00702916	0,00984285	0,01251610	0,01517225	0,01789495	0,02076193		0,02386362	0,02732369	0,03133445	0,03623529	0,04272850	0,05267985	0,06657109		
0,00141843	0,00508811	0,00802613	0,01068546	0,01325087	0,01581658	0,01845240	0,02122575		0,02421556	0,02752833	0,03132503	0,03587795	0,04171435	0,05008097	0,06525629		
0,00260377	0,00582273	0,00861647	0,01119302	0,01369718	0,01620996	0,01879419	0,02151175		0,02443529	0,02766200	0,03133651	0,03569758	0,04119113	0,04881004	0,06155832		
0,00289596	0,00616019	0,00889338	0,01143301	0,01390909	0,01639724	0,01895729	0,02164865		0,02454117	0,02772791	0,03134633	0,03562092	0,04096415	0,04827062	0,06011100		

Figure 3-13. B calculation for initially shown sliding rate.

4. And finally the tangential effort:

					0	0	0	0	0	0	0						
			0	0	0,000839566	0,005313912	0,010412795	0	0,014949465	0,017633159	0,015343791	0	0				
		0	0,000487525	0,005895685	0,011222426	0,017033925	0,022764569	0	0,028202362	0,033078716	0,036938891	0,041005219	0,026406957	0			
	0	0,001162874	0,006643386	0,012651338	0,018873945	0,025119956	0,031242388	0	0,037093039	0,042488908	0,047160065	0,050623145	0,051726557	0,041442642	0		
0	0,000340718	0,005654939	0,011758731	0,018173717	0,024699598	0,031203339	0,037569581	0	0,043677742	0,049381427	0,054477330	0,058640100	0,061244021	0,060645310	0,037216430		
0	0,003516796	0,009284330	0,015725236	0,022376721	0,029093364	0,035766208	0,042295698	0	0,048576206	0,054480904	0,059839363	0,064394185	0,067696730	0,068777599	0,068306547	0	
0,000293993	0,005709024	0,011986494	0,018622497	0,025421359	0,032261441	0,039046115	0,045684699	0	0,052080294	0,058117377	0,063643692	0,068436741	0,072128809	0,073996856	0,072103649	0,042197073	
0,001484729	0,007326613	0,013770177	0,020518466	0,027405239	0,034320450	0,041174009	0,047880181	0	0,054347028	0,060465417	0,066093098	0,071026004	0,074936544	0,077211282	0,076364238	0,061902003	
0,002214295	0,008138340	0,014655956	0,021456194	0,028384351	0,035335291	0,042221812	0,048960420	0	0,055461449	0,061618676	0,067294351	0,072292516	0,076302672	0,078755673	0,078328912	0,069173685	
0	0	0	0	0	0	0	0	0	0	0	0	0	0	0	0	0	0

Figure 3-14. F_T calculation for initial shown data for circular contact shape, on each asperity.

To get the overall, in term of a sliding ration, it is not different from what has been done. It's only need to sum every asperity value, shown above, and then multiply it by 2.

Hereafter, it is only required to do the same procedure as previously done, which is changing the sliding rate to get new F_T. so it is possible to plot the data, which is shown below:

Table 3.7. Distance covered by each corpse for Δt.

ΔV/Vr (%)	∑ Ft	∑ Ft / (Fn . μ)
0,001000005	7,751355234	0,037996839
0,00200002	15,343781490	0,075214615
0,005000125	37,073913963	0,181734872
0,00800032	57,106077306	0,279931752
0,0100005	69,523114576	0,340799581
0,020002	119,783598657	0,587174503
0,050012503	179,681693879	0,880792617
0,070024509	190,731272294	0,934957217
0,100050025	197,254395280	0,96693331
0,2002002	202,100425533	0,99068836
0,501253133	203,451847846	0,99731298
0,803212851	203,518551855	0,99763996
1,005025126	203,518551855	0,99763996
2,02020202	203,518551855	0,99763996

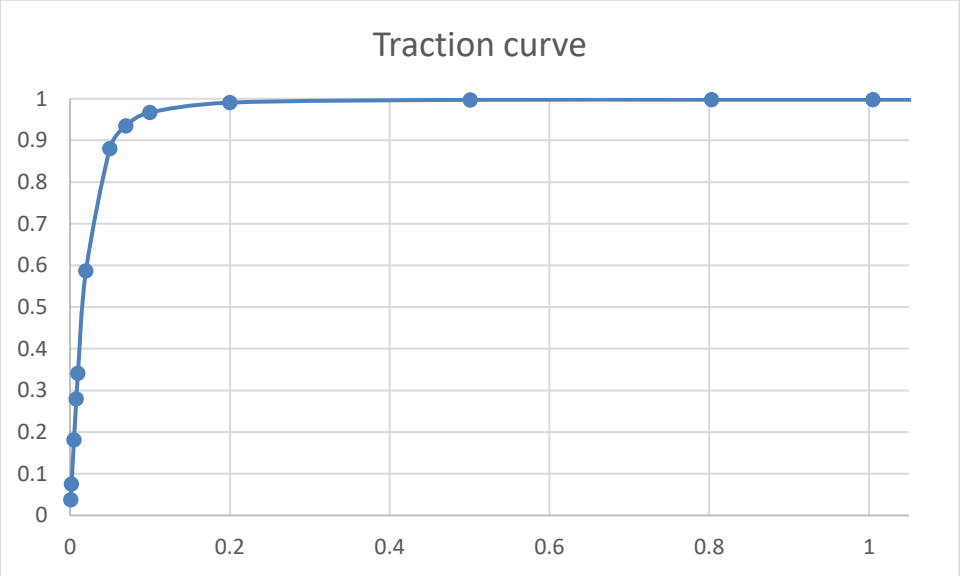

Figure 3-15. Traction curve.

3.2. Practical study

As many times mentioned, the aim of this dissertation is to compare theoretical study with some pratical experiences values for adhesion ratio, and for this reason it is necessary to explain the way in which it was made. It is important to keep in mind that these experiences were made in SUPMECA by E. Cullaz, M. Quillien. F.Robbe-Valloire and F. Macewko.

The pratical experience of this non lubricated rolling/sliding contact were done in a twin-disc aparatus

[BIBLIOGRAPHY]

[1]. D.Dowson,(1969) Tribology- Inaugural Lectura. Univesity of Leeds Press,.

[2]. J.Halling, Principles of Tribology, MacMillian, 1975.

[3]. F.Al-Bender, K. De Moerlooze, On the relationship between normal load and friction force in pre-sliding frictional contacts. Part1: Theoretical analysis, 2010

[4]. G.A.Tomlinson, A molecular theory of friction, Philosophical Magazine Series 7(7), (1929) 905-939

[5]. T.Baumberger, Chapter 1. Dry friction dynamics at low velocities, in: Physics of Sliding Friction, Kluwer Academic Publishers, 1996, pp. 1-16

[6]. M.Weiss, F.J. Elmer, Dry friction in the Frenkel-k

[7]. M. Weiss, F.J. Elmer, Dry friction in the Frenkel–Kontorova–Tomlinson model: dynamicalproperties, Zeitschrift für Physik B:CondensedMatter104(1) (1997) 55–69.

[8]. B.N.J. Persson, O. Albohr, F. Mancosu, V. Peveri, V.N. Samoilov, I.M. Sivebaek, On the nature of the static friction, kinetic friction and creep, Wear 254 (2003) 835–851

[9]. F. Al-Bender, V. Lampaert, J. Swevers, A novel generic model at asperity level for dry friction force dynamics, Tribology Letters 16 (1) (2004) 81–93

[10]. Bureau, L., Caroli, C., & Baumberger, T. (2003). Elasticity and onset of frictional dissipation at a non − sliding multi − contact interface Elasticity and onset of frictional dissipation, 2787–2805

[11]. Mindlin, R. D., Mason, W. P., Osmer, T. F. & Deresiewicz, H. 1951 effects of an oscillating force on the contact surfaces of elastic spheres. In Proc. 1st US Nat. Congr. in Applied Mechanics, pp. 203{208.

[12]. Johnson, K. L. 1955 Surface interaction between elastically loaded bodies under tangential forces. Proc. R. Soc. Lond. A230, 531-549.

[13]. Johnson, K. L. 1961 Energy dissipation at spherical surfaces in contact transmitting oscillatiing forces. J. Mech. Sci. 3, 362.

[14]. A. E. H. Love, A Treatise on the Mathematical Theory of Elasticity Cambridge University Press, Cambridge, 1926.

[15]. K. L. Johnson, Contact Mechanics, Cambridge University Press, Cambridge, 1985.

[16]. Kalker, J.J. (1991), Wheel-Rail contact theory, 243-261

[17]. Williams, John A, Contact Between Solid Surfaces,

[18]. Carter, F.W., On the action of locomotive driving Wheel, Proceeding of the Royal Society of London, A112, 1926, p.151-157.

[19]. Stefan Björklund, The influence of surface roughness in elliptical contacts

[20]. Archard, J.F. , 1957. Elastic deformation and the laws of friction. Proc. R. Soc. A 243, 190–205.

[21]. J.A. Greenwood and J.B.P. Williamson. Contact of nominally flat surfaces. Proceedings of the Royal Society of London. Series A., 295:300–319, 1966.

[22]. P.R. Nayak. Random process model of rough surfaces in plastic contact. Wear, 26:305–333,1973.

[23]. M.S. Longuet-Higgins. The statistical analysis of a random, moving surface. Philosophical Transactions of Royal Society of London. Series A, 249: 321-287,1957.

[24]. Lim, C.W. , Li, Z.R. , He, L.H. , 2006. Size dependent, non-uniform elastic field inside a nano-scale spherical inclusion due to interface stress. Int. J. Solids Struct. 43, 5055–5065

[25]. Huang, Z.P. , Sun, L. , 2007. Size-dependent effective properties of a heterogeneous material with interface energy effect: from finite deformation theory to in- finitesimal strain analysis. Acta Mech. 190, 151–163 .

[26]. Ru, C.Q. , 2009. Size effect of dissipative surface stress on quality factor of mi- crobeams. Appl. Phys. Lett. 94, 051905.

[27]. Wang, G.F. , Feng, X.Q. , 2009. Timoshenko beam model for buckling and vibration of nanowires with surface effects. J. Phys. D: Appl. Phys. 42, 15541 .

[28]. Olsson, P.A.T. , Park, H.S. , 2012. On the importance of surface elastic contributions to the flexural rigidity of nanowires. J. Mech. Phys. Solids 60, 2064–2083 .

[29]. Weike Yuan ,Jianmin Long, Yue Ding, Gangfeng Wang, Statistical contact model of rough surfaces: The role of surface tension.

[30]. Antonis I. Vakis, 2014, Asperity Interaction and Substrate Deformation in Statistical Summation Models of Contact Between Rough Surfaces , 1-10.

[31]. Paggi, M., and Ciavarella, M., 2010, “The Coefficient of Proportionality K Between Real Contact Area and Load, With New Asperity Models,” Wear, 268(7–8), pp. 1020–1029

[ANNEX A]

Data										
	Main values for variation									
Radius differences (mm):	20									
E1 differences (Gpa):	30									
N1 differences (N):	50									
E2 differences (Gpa) :	30									
1st Situation. Ball-Flat Plan										
Ball features :	Initial data:	Changing parameter:								
Radii (mm)	100	120	120	120	120	120	120	120	120	120
Young Modulus E1 (GPa)	270	300	330	360	390	420	450	480	510	540
Load applied (N)	1000	1050	1100	1150	1200	1250	1300	1350	1400	1450
Plan features :										
Young Modulus E2 (GPa)	100	130	160	190	220	250	280	310	340	370

Figure AP 0-1. Initial data, increment and changing parameters.

Parameteres to be evaluated in different situations	(1) Increasing E1, Linear E2									
Constant Load	1000									
Constant radii	100									
$E'=$	72,97297297	75	76,744186	78,2608696	79,5918367	80,7692308	81,8181818	82,7586207	83,6065574	84,375
displacement (mm)- δ	1,018433826	1	0,98479051	0,97202566	0,96115882	0,95179527	0,94364279	0,93648037	0,93013777	0,9244817
contact area between surfaces (mm2) - A	319,9504227	314,159265	309,381062	305,370867	301,95695	299,015304	296,454126	294,203986	292,211399	290,434491

Figure AP 0-2. Displacement and contact area changes when increasing E_1 and remaining E_2 constant.

Parameteres to be evaluated in different situations	(2) Increasing Load									
$E'=$	72,97297297									
Increasing Load	1000	1050	1100	1150	1200	1250	1300	1350	1400	1450
Constant Radii	100									
displacement (mm)- δ	1,018433826	1,05210483	1,08524536	1,11788735	1,15005951	1,18178777	1,21309566	1,24400462	1,27453424	1,30470247
contact area between surfaces (mm2) - A	319,9504227	330,528481	340,939886	351,194669	361,30185	371,269577	381,105243	390,815579	400,406739	409,884369

Figure AP 0-3. Increasing load.

Parameteres to be evaluated in different situations	(3) Increasing sphere radius									
$E' = (1/E1 + 1/E2)^{-1}$	72,97297297									
Constant Load	1000									
Increasing Radii	100	120	140	160	180	200	220	240	260	280
displacement (mm)- δ	1,018433826	0,95838292	0,9103816	0,87074867	0,8372246	0,80833146	0,78305438	0,76066903	0,74064205	0,72257035
contact area between surfaces (mm2) - A	319,9504227	361,30185	400,406739	437,686022	473,439357	507,889638	541,208334	573,530937	604,966863	635,606079

Figure 0-4. Increasing sphere radius.

Reference Stiffness (K_{ref})	1472,849744									
1st case: 1 circle Increasing radii										
k	1472,849744	1565,1364	1647,66072	1722,65551	1791,63393	1855,6744	1915,57578	1971,9483	2025,26983	2075,92243
2nd case: N circles smaller radii										
number of circles - n	1	2	3	4	5	6	7	8	9	10
radius decrease	100	50	33,3333333	25	20	16,6666667	14,2857143	12,5	11,1111111	10
Total displacement - δ (mm)	1,018433826	0,80833146	0,70614258	0,64157311	0,59558371	0,56046573	0,53239439	0,50921691	0,48961192	0,47271511
k (each circle) (N/mm)	1472,849744	927,837198	708,072303	584,500808	503,707527	446,0576	402,494315	368,212436	340,405658	317,315858
k (Whole sistem) (N/mm)	1472,849744	1855,6744	2124,21691	2338,00323	2518,53763	2676,3456	2817,4602	2945,69949	3063,65093	3173,15858

Figure AP 0-5. Stiffness evaluation.

Cylinder	1	2
v -poisson ratio	0,3	0,3
C-Modulus of rigidity - [Mpa]	79300	79300
μ- friction ratio	0,3	
Length - L [mm]	10	
Fn-Normal Force - [N/mm]	400	
Normal Force - [N]	4000	
E - Young Modulus [Mpa]	210000	210000
E' [MPa]	115384,6154	
Radius [mm]	5	5
R' [mm]	2,5	
a2 - square width of contact - [mm2]	0,054454273	
2a - width of contact [mm]	0,466708786	
P(x) [N/mm2]	P(X)	
p0 [N/mm2]	1091,24969	
Asperity radius - r [mm]	0,02	0,02
Equivalent asperity radius - r' [mm]	0,01	
Asperity periodicity - p [mm]	0,05	
number of asperitys [length]- n	200	
number of asperitys [width] - n	9,334175714	
Angular velocity [rad/s]	77	76,9846
V [m/s]	0,385	0,384923
V [mm/s]	385	384,923
Vr	384,9615	
ΔV	0,077	
ΔV/Vr	0,00020002	
ΔV/Vr (%)	0,020002	

Figure AP 0-6. Cylinder-cylinder contact data.

						0,379967	0,3929058	0,399217986	0,4	0,3992	0,39290584	0,3799671						
				0,33071891	0,35968736	0,375	0,375	0,375	0,375	0,375	0,375	0,375	0,35968736	0,3307189				
			0,29047375	0,325	0,325	0,325	0,325	0,325	0,325	0,325	0,325	0,325	0,325	0,325	0,2904738			
		0,233184476	0,275	0,275	0,275	0,275	0,275	0,275	0,275	0,275	0,275	0,275	0,275	0,275	0,275	0,23318448		
		0,225	0,225	0,225	0,225	0,225	0,225	0,225	0,225	0,225	0,225	0,225	0,225	0,225	0,225	0,225		
	-0,13919	0,175	0,175	0,175	0,175	0,175	0,175	0,175	0,175	0,175	0,175	0,175	0,175	0,175	0,175	0,175	0,13919	
0,125	0,125	0,125	0,125	0,125	0,125	0,125	0,125	0,125	0,125	0,125	0,125	0,125	0,125	0,125	0,125	0,125	0,125	0,125
0,075	0,075	0,075	0,075	0,075	0,075	0,075	0,075	0,075	0,075	0,075	0,075	0,075	0,075	0,075	0,075	0,075	0,075	0,075
0,025	0,025	0,025	0,025	0,025	0,025	0,025	0,025	0,025	0,025	0,025	0,025	0,025	0,025	0,025	0,025	0,025	0,025	0,025
0	0	0	0	0	0	0	0	0	0	0	0	0	0	0	0	0	0	0
-0,025	-0,025	-0,025	-0,025	-0,025	-0,025	-0,025	-0,025	-0,025	-0,025	-0,025	-0,025	-0,025	-0,025	-0,025	-0,025	-0,025	-0,025	-0,025
-0,075	-0,075	-0,075	-0,075	-0,075	-0,075	-0,075	-0,075	-0,075	-0,075	-0,075	-0,075	-0,075	-0,075	-0,075	-0,075	-0,075	-0,075	-0,075
-0,125	-0,125	-0,125	-0,125	-0,125	-0,125	-0,125	-0,125	-0,125	-0,125	-0,125	-0,125	-0,125	-0,125	-0,125	-0,125	-0,125	-0,125	-0,125
	-0,13919	-0,175	-0,175	-0,175	-0,175	-0,175	-0,175	-0,175	-0,175	-0,175	-0,175	-0,175	-0,175	-0,175	-0,175	-0,175	-0,1391941	
		-0,225	-0,225	-0,225	-0,225	-0,225	-0,225	-0,225	-0,225	-0,225	-0,225	-0,225	-0,225	-0,225	-0,225	-0,225		
		-0,23318448	-0,275	-0,275	-0,275	-0,275	-0,275	-0,275	-0,275	-0,275	-0,275	-0,275	-0,275	-0,275	-0,275	-0,23318448		
			-0,2904738	-0,325	-0,325	-0,325	-0,325	-0,325	-0,325	-0,325	-0,325	-0,325	-0,325	-0,325	-0,2904738			
				-0,3307189	-0,3596874	-0,375	-0,375	-0,375	-0,375	-0,375	-0,375	-0,375	-0,3596874	-0,3307189				
						-0,37997	-0,392906	-0,399217986	-0,4	-0,3992	-0,3929058	-0,3799671						

Figure AP 0-7. Asperities Z values, on circular contact shape.

						-0,125	-0,075	-0,025	0	0,025	0,075	0,125						
				-0,18919	-0,139	-0,125	-0,075	-0,025	0	0,025	0,075	0,125	0,175	0,225				
			-0,23318	-0,225	-0,175	-0,125	-0,075	-0,025	0	0,025	0,075	0,125	0,175	0,225	0,275			
		-0,29	-0,275	-0,225	-0,175	-0,125	-0,075	-0,025	0	0,025	0,075	0,125	0,175	0,225	0,275	0,325		
	-0,330718914	-0,325	-0,275	-0,225	-0,175	-0,125	-0,075	-0,025	0	0,025	0,075	0,125	0,175	0,225	0,275	0,325		
	-0,359687364	-0,325	-0,275	-0,225	-0,175	-0,125	-0,075	-0,025	0	0,025	0,075	0,125	0,175	0,225	0,275	0,325	0,375	
-0,3799671	-0,375	-0,325	-0,275	-0,225	-0,175	-0,125	-0,075	-0,025	0	0,025	0,075	0,125	0,175	0,225	0,275	0,325	0,375	0,37997
-0,39290584	-0,375	-0,325	-0,275	-0,225	-0,175	-0,125	-0,075	-0,025	0	0,025	0,075	0,125	0,175	0,225	0,275	0,325	0,375	0,39291
-0,39921799	-0,375	-0,325	-0,275	-0,225	-0,175	-0,125	-0,075	-0,025	0	0,025	0,075	0,125	0,175	0,225	0,275	0,325	0,375	0,39922
-0,4	-0,375	-0,325	-0,275	-0,225	-0,175	-0,125	-0,075	-0,025	0	0,025	0,075	0,125	0,175	0,225	0,275	0,325	0,375	0,4
	-0,375	-0,325	-0,275	-0,225	-0,175	-0,125	-0,075	-0,025	0	0,025	0,075	0,125	0,175	0,225	0,275	0,325	0,375	
	-0,375	-0,325	-0,275	-0,225	-0,175	-0,125	-0,075	-0,025	0	0,025	0,075	0,125	0,175	0,225	0,275	0,325	0,375	
	-0,375	-0,325	-0,275	-0,225	-0,175	-0,125	-0,075	-0,025	0	0,025	0,075	0,125	0,175	0,225	0,275	0,325	0,375	
	-0,375	-0,325	-0,275	-0,225	-0,175	-0,125	-0,075	-0,025	0	0,025	0,075	0,125	0,175	0,225	0,275	0,325	0,375	
		-0,325	-0,275	-0,225	-0,175	-0,125	-0,075	-0,025	0	0,025	0,075	0,125	0,175	0,225	0,275	0,325		
		-0,325	-0,275	-0,225	-0,175	-0,125	-0,075	-0,025	0	0,025	0,075	0,125	0,175	0,225	0,275	0,325		
			-0,275	-0,225	-0,175	-0,125	-0,075	-0,025	0	0,025	0,075	0,125	0,175	0,225	0,275			
				-0,225	-0,175	-0,125	-0,075	-0,025	0	0,025	0,075	0,125	0,175	0,225				
						-0,125	-0,075	-0,025	0	0,025	0,075	0,125						

Figure AP 0-8. Asperities X values, on circular contact shape.

					0	0	0	0	0	0	0					
			0	0	310,6604442	594,8694612	694,6578712	706,1405974	694,6578712	594,8694612	310,6604442	0	0			
		0	310,6604442	781,8116399	998,6336098	1120,102161	1176,14146	1182,959728	1176,14146	1120,102161	998,6336098	781,8116399	310,6604442	0		
	0	474,5416671	931,9813327	1176,14146	1330,168553	1423,625001	1468,123982	1473,591874	1468,123982	1423,625001	1330,168553	1176,14146	931,9813327	474,5416671	0	
	310,6604442	931,9813327	1229,629463	1423,625001	1553,302221	1634,046375	1672,957691	1677,758154	1672,957691	1634,046375	1553,302221	1423,625001	1229,629463	931,9813327	310,6604442	
0	781,8116399	1176,14146	1423,625001	1594,185583	1710,984313	1784,608384	1820,304086	1824,716951	1820,304086	1784,608384	1710,984313	1594,185583	1423,625001	1176,14146	781,8116399	0
310,6604442	998,6336098	1330,168553	1553,302221	1710,984313	1820,304086	1889,67371	1923,42055	1927,597364	1923,42055	1889,67371	1820,304086	1710,984313	1553,302221	1330,168553	998,6336098	310,6604442
594,8694612	1120,102161	1423,625001	1634,046375	1784,608384	1889,67371	1956,585417	1989,19742	1993,236404	1989,19742	1956,585417	1889,67371	1784,608384	1634,046375	1423,625001	1120,102161	594,8694612
694,6578712	1176,14146	1468,123982	1672,957691	1820,304086	1923,42055	1989,19742	2021,28332	2025,258315	2021,28332	1989,19742	1923,42055	1820,304086	1672,957691	1468,123982	1176,14146	694,6578712
706,1405974	1182,959728	1473,591874	1677,758154	1824,716951	1927,597364	1993,236404	2025,258315	2029,225524	2025,258315	1993,236404	1927,597364	1824,716951	1677,758154	1473,591874	1182,959728	706,1405974

Figure AP 0-9. Pressure distribution on circular contact shape.

[ANNEX B]

Table AP 0.1. Asperity width based on Johson's article.

	JOHNSON ARTICLE
Fn(per asperity)	Asperity width - a(i)
0	0
0,048260225	0,001464804
0,180469392	0,002273619
0,23037099	0,002466375
0,258337998	0,002562394
0,271242299	0,002604368
	0
0,271242299	0,002604368
0,258337998	0,002562394
0,23037099	0,002466375
0,180469392	0,002273619
0,048260225	0,001464804
0	0

Table AP 0.2. Normal force calculation based on rectangular áreas, contact between cylinders.

x(asperity position)	P(x)	Fn(per column)	Fn(per asperity
-0,233354393	0	0	0
-0,225	289,3785248	9,652044998	0,048260225
-0,175	721,8775671	36,09387836	0,180469392
-0,125	921,483961	46,07419805	0,23037099
-0,075	1033,35199	51,66759952	0,258337998
-0,025	1084,969197	54,24845986	0,271242299
0	1091,24969		
0,025	1084,969197	54,24845986	0,271242299
0,075	1033,35199	51,66759952	0,258337998
0,125	921,483961	46,07419805	0,23037099
0,175	721,8775671	36,09387836	0,180469392
0,225	289,3785248	9,652044998	0,048260225
0,233354393	0	0	0

Table AP 0.3. Distance covered by each corpse for $V_i \cdot \Delta t$.

$X_1 = V_1 \text{x } \Delta t$	$X_2 = V_2 \text{x } \Delta t$	$\Delta X = \lvert X_1 - X_2 \rvert$
Distance covered (mm)	**Distance covered (mm)**	**Distance between asperity center of mass**
0,008355229	0,008353557	1,67105E-06
0,058360229	0,058348557	1,1672E-05
0,10836523	0,108343556	2,1673E-05
0,15837023	0,158338556	3,1674E-05
0,208375231	0,208333555	4,1675E-05
0,258380231	0,258328555	5,1676E-05
0,308385232	0,308323554	6,1677E-05
0,358390232	0,358318554	7,1678E-05
0,408395233	0,408313553	8,1679E-05
0,458400233	0,458308553	9,168E-05

Table AP 0.4. F_T for asperity, column and overall summation.

Per asperity	**Per column**
F_T = (1-Y)* μF_N	F_T
0	0
0,000454267	0,090853476
0,004874896	0,974979155
0,009729023	1,94580464
0,014637901	2,927580161
0,019385068	3,877013633
0,023769763	4,75395267
0,027528304	5,505660888
0,03020028	6,040055993
0,030635003	6,12700069
0,014478067	2,895613499
TOTAL SHEAR FORCE	35,13851481

Table AP 0.5. Main data for circular contact shape. Experiences made in SUPMECA.

Body	Cylinder	Cylinder
σ -poisson ratio	0,3	0,3
Modulus of rigidity - C [Mpa]	73000	73000
friction ratio - μ	0,3	
Normal Force - N [N/mm]	680	
Young Modulus - E [Mpa]	210000	210000
E' [MPa]	115384,6154	
Semi-major half width of contact - a [mm]	0,4	
Semi-minor half width of contact - b [mm]	0,4	
P[x,z) [N/mm2]	P(X,Z)	
Maximum contact pressure - p0 [MPa]	2029,225524	
Radius i [mm]	15	15
Equivalent radius R' [mm]	7,5	
Asperity radius [mm]	0,02	0,02
Equivalent asperity radius	0,01	
Asperity periodicity - p [mm]	0,05	0
number of asperitys [length) - n	68,56524021	0
number of asperitys [width) - n	0	0
Angular velocity [rpm]	7	6,99993
V [m/s]	0,105	0,10499895
V [mm/s]	105	104,99895
Vr	104,999475	
ΔV	0,00105	
ΔV/Vr	1,00001E-05	
ΔV/Vr (%)	0,001000005	

[APPENDIX A]

[Remover se necessário para garantir que o próximo Capítulo inicia numa página ímpar]

[APPENDIX B]